Journal of Sound and Vibration 374 (2016) 260–278

Contents lists available at ScienceDirect

Journal of Sound and Vibration

journal homepage: www.elsevier.com/locate/jsvi

Transmission and reflection of acoustic and entropy waves through a stator–rotor stage

Michael Bauerheim [a], Ignacio Duran [b], Thomas Livebardon [b], Gaofeng Wang [c], Stéphane Moreau [c,*], Thierry Poinsot [d]

[a] LMFA, Ecole Centrale de Lyon, 36 Avenue Guy de Collongue, 69130 Ecully, France
[b] CERFACS, 31057 Toulouse, France
[c] Université de Sherbrooke, Sherbrooke, QC, Canada J1K2R1
[d] Institut de Mécanique des Fluides de Toulouse, 31400 Toulouse, France

ARTICLE INFO

Article history:
Received 4 January 2016
Received in revised form
30 March 2016
Accepted 31 March 2016
Handling Editor: Y. Auregan
Available online 15 April 2016

ABSTRACT

The propagation of acoustic, entropy and vorticity waves through turbine stages is of significant interest in the field of core noise. In particular, entropy spots have been shown to generate significant noise when accelerated through turbine stages: the so-called indirect combustion noise. Analytical models for the propagation of acoustic, vorticity and entropy waves through a stator vane, developed since the seventies, are generally based on restrictive assumptions such as low frequency waves. In order to analyze such assumptions, the theory of Cumpsty and Marble is extended to rotating rows and applied to a 2D stator–rotor turbine stage. The theoretical transfer functions are then compared with numerical predictions from forced compressible Large-Eddy Simulations of a 2D stator–rotor configuration, using a fluid–fluid coupling strategy with an overset-grid method. The comparisons between the analytical model and the simulations are in good agreement. To improve the analytical predictions, the attenuation due to the entropy spot deformation through the stator vane or the rotor blade is then included, modeled either analytically or extracted from the mean flow of the simulations. The complete analytical model reveals a good agreement with 2D simulations, which allows the prediction and minimization of both direct and indirect noise at the design-stage without computation.

1. Introduction

The International Civil Aviation Organization (ICAO) predicts a significant increase of air traffic, the latter doubling in the next two decades. Consequently the environmental impact of airplanes will be even more regulated and stricter limitations on noise and pollutant emissions imposed to aircraft manufacturers by ICAO. Since the first investigations by Lighthill [27], the reduction of aircraft noise has been continuously focused on the main aerodynamic sources: jet, fan, turbomachinery and airframe noise. With mainly the constant increase of the by-pass ratio of turboengines, these sources have been significantly reduced over the last decades. Other sources such as combustion noise have seen their relative influence increase over the last years not only because of the aforementioned global reduction of engine noise but also because of shorter, more highly loaded turbines that do not shield it as efficiently, and also the development of new low NO_x-emission

* Corresponding author.
E-mail address: Stephane.Moreau@USherbrooke.ca (S. Moreau).

http://dx.doi.org/10.1016/j.jsv.2016.03.041
0022-460X/

combustion chambers such as lean premixed, rich-quench-lean or staged-injection combustion chambers in which larger turbulent fluctuations lead to unsteady heat release and more noise generation.

Marble and Candel [31] and Cumpsty and Marble [9] showed that there are two main mechanisms of combustion noise generation that propagate through the turbine stages to the outlet of the engine: the direct and indirect combustion noise. The former is caused by the acoustic waves generated by the unsteady heat release of turbulent combustion. This mechanism has been studied by Strahle [40,41] and more recently by Ihme and Pitsch [19] for instance. The latter, also called entropy noise, is caused by the convection of entropy waves, or hot-spots, through turbine stages. When these entropy spots are accelerated in the turbine rows, they generate acoustic waves, a mechanism which has been studied by Marble and Candel [31], Cumpsty and Marble [9], Bake et al. [3], Leyko et al. [25,26] and Howe [18]. In some cases, depending on the outlet conditions of the combustion chamber, entropy noise was thought to be larger than direct noise [6,34,35]. Analytically, Leyko et al. [25] showed with a 1D model combustor with a choked nozzle that indirect noise can be one order of magnitude larger than direct noise in actual turbo-engines and negligible in existing laboratory experiments. More recently, this noise mechanism was experimentally shown to be relevant in auxiliary power units [42] and helicopter engines [4,28].

Combustion noise is therefore strongly connected with the propagation of acoustic and entropy waves through the turbine stages. In the case of direct noise, the propagation through turbine rows contributes to the noise attenuation while in the case of the indirect mechanism, noise is produced during the propagation of the entropy wave through an accelerating flow. Marble and Candel [31] developed a first analytical method to predict the noise generated at the outlet of a 1D nozzle by acoustic and entropy waves. This analytical solution is based on the compact nozzle assumption, in which the wavelengths of the perturbations are assumed to be much larger than the 1D nozzle dimensions, limiting the results to the very low frequency range. Jump conditions can then be written between the inlet and the outlet of the compact nozzle for the mass, total temperature and entropy fluctuations. By comparing with the experimental data of Bake et al. [3], such a 1D analytical model was validated by Leyko et al. [26] in the case of a supersonic flow, and by Duran et al. [14] in the subsonic case. The validity of the compact nozzle hypothesis has been investigated numerically [1,22,15], and analytical modeling has been extended for non-compact frequencies [13,16,17,39].

Based on 1D models, several analytical and semi-analytical models have been extended to predict the propagation of acoustic waves through turbine blades in 2D configurations such as those developed by Muir [32,33] and Kaji and Okazaki [20,21]. Yet, all these models only consider acoustic and vorticity waves, neglecting entropy fluctuations and therefore indirect noise. To include the additional effect of entropy waves, Cumpsty and Marble [9] extended the aforementioned 1D analytical model of Marble and Candel [31] to a stator vane in a 2D configuration at midspan accounting for the significant effect of flow deviation in a turbine, and including vorticity waves through the stator vane. This method was compared by Leyko et al. [24,23] with numerical simulations for the case of a stator vane showing that the compact low-frequency limit of the analytical method predicted correctly the transfer functions (both the reflected and transmitted acoustic waves) generated by acoustic and entropy waves. For the case of direct noise, the compact solution was shown to be valid over a wide range of frequencies. For the case of indirect noise however, the entropy wave was shown to be strongly deformed by the presence of the stator blade. The indirect noise was nevertheless shown to be correctly predicted at low frequencies, which are dominant in combustion noise.

In this context, the goal of the present study is to extend the previous work of Leyko et al. [24,23] to the propagation of waves through a complete realistic turbine stage, containing both a stator and a rotor. The 2D analytical model of Cumpsty and Marble [9] is first explained in Section 2, and then extended to take into account the effect of the rotor blade. This yields a complete propagation model through a full compact multi-stage turbomachinery termed CHORUS. Detailed numerical unsteady simulations are then performed to obtain reference transfer functions at all frequencies to validate the analytical results. The set-up of these simulations is explained in Section 3 and results are discussed in Section 4. A new analytical indirect noise model is proposed based on a modeled axial velocity profile yielding an analytical formulation of the attenuation of entropy waves through a turbine row, and a parametric study is undertaken. Conclusions are finally drawn in Section 5.

2. Analytical method

The analytical method developed by Cumpsty and Marble [9] to predict the wave propagation through stator blades is first recast in matrix form and extended to rotating blades. The model relies on the compact assumption, which considers that the wavelengths of the perturbations are greater than the axial length of the turbine stages. With this assumption, the acoustic and entropy waves propagate quasi-steadily through the turbine stages, and jump conditions can be simply written between the inlet and the outlet of each turbine row. A 2D blade-to-blade configuration is considered (any radial variation are omitted), and the flow upstream and downstream of each blade row is assumed steady and uniform (mean speed triangles at the mean radius R of the meridian plane of the turbine). Fig. 1 shows a sketch of such a configuration: an infinitely thin blade row behaves as an interface between two regions of uniform flow. $\overline{\mathbf{w}}$ represents the mean relative flow-velocity vector (with module $\overline{w}$ and an angle $\overline{\theta}$ with the axial direction), and $\mathbf{k}$ is the wave vector that provides the propagation direction of the considered wave (similarly with module k and angle ν with the axial direction).

The mean flow is described by four variables: $\overline{w}$, $\overline{\theta}$, the mean pressure $\overline{p}$ and the mean density of the flow $\overline{\rho}$. This mean flow is perturbed by small fluctuations, which can be described by four primitive variables: the entropy perturbation s', the relative-velocity perturbation w', the pressure fluctuation p', and the perturbation of the flow angle θ'.

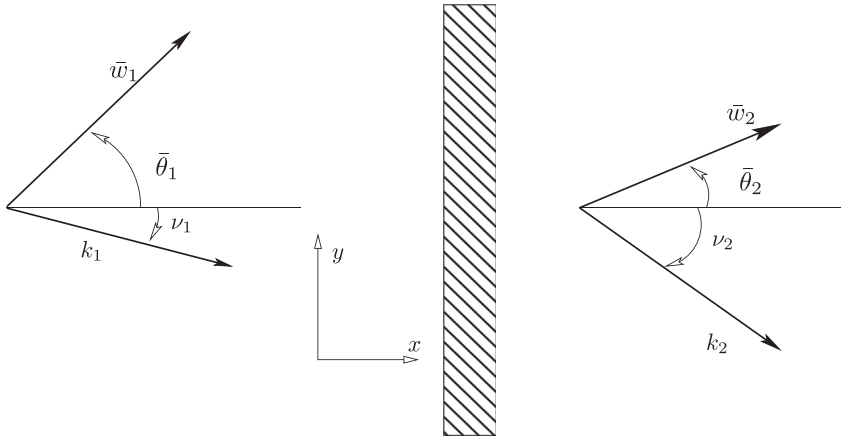

Fig. 1. Sketch of the studied configuration.

The compact analytical method provides the wave propagation upstream and downstream of the blade row, where the flow is considered steady and homogeneous. The acoustic, entropy and vorticity waves are first related to the dimensionless primitive fluctuating variables s'/Cp, $w'/\overline{c}$, $p'/\gamma\overline{p}$ and θ' (Section 2.1). In a second step, four matching conditions at the interfaces between the upstream and downstream regions of a turbine row are obtained (Section 2.2).

2.1. Wave decomposition

The fluctuating primitive variables are related to the propagating waves by the 2D linearized Euler equations (LEE) in a steady uniform flow as in Cumpsty and Marble [9]. The latter equations are obtained by linearization of the 2D Euler equations around a mean steady homogeneous flow, and are therefore limited to the inter-blade regions. They read

$$\frac{\mathrm{D}}{\mathrm{D}t}\left(\frac{\rho'}{\overline{\rho}}\right)+\frac{\partial u'}{\partial x}+\frac{\partial v'}{\partial y}=0, \tag{1}$$

$$\frac{\mathrm{D}}{\mathrm{D}t}(u')=-\frac{1}{\overline{\rho}}\frac{\partial p'}{\partial x}, \tag{2}$$

$$\frac{\mathrm{D}}{\mathrm{D}t}v'=-\frac{1}{\overline{\rho}}\frac{\partial p'}{\partial y}, \tag{3}$$

$$\frac{\mathrm{D}}{\mathrm{D}t}\left(\frac{s'}{C_p}\right)=\frac{\mathrm{D}}{\mathrm{D}t}\left(\frac{p'}{\gamma\overline{p}}-\frac{\rho'}{\overline{\rho}}\right)=0, \tag{4}$$

where

$$\frac{\mathrm{D}}{\mathrm{D}t}=\frac{\partial}{\partial t}+\overline{\mathbf{w}}\cdot\nabla=\frac{\partial}{\partial t}+\overline{u}\frac{\partial}{\partial x}+\overline{v}\frac{\partial}{\partial y} \tag{5}$$

stands for the substantial derivative, $\overline{u}=\overline{w}\cos\overline{\theta}$ and $\overline{v}=\overline{w}\sin\overline{\theta}$ for the axial and tangential components of the mean relative velocity respectively. u' and v' are the velocity fluctuating variables in the x and y directions respectively. They can be related to the other fluctuations w' and θ' by simple trigonometric relations,

$$\frac{u'}{\overline{u}}=\frac{w'}{\overline{w}}-\theta'\tan\overline{\theta},\quad \frac{v'}{\overline{v}}=\frac{w'}{\overline{w}}+\theta'/\tan\overline{\theta}. \tag{6}$$

The system of equations given in (1)–(4) can also describe the wave propagation in a two-dimensional steady homogeneous flow. Any wave ϕ can be considered as harmonic and monochromatic

$$w^{\phi}=A_{\phi}\exp\left[-\mathrm{i}(\omega t-\mathbf{k}_{\phi}\cdot\mathbf{x})\right], \tag{7}$$

where A_{ϕ} represents its amplitude, ω the angular frequency, $\mathbf{x}$ the vector in the fixed reference frame, t the time, and $\mathbf{k}_{\phi}$ the wave vector that can be expressed as a combination of axial and tangential components,

$$\mathbf{k}_{\phi}\cdot\mathbf{x}=\mathbf{k}_{\phi,x}\mathbf{x}+\mathbf{k}_{\phi,y}\mathbf{y},\quad \text{with } \mathbf{k}_{\phi,x}=\mathbf{k}_{\phi}\cos\nu_{\phi} \text{ and } \mathbf{k}_{\phi,y}=\mathbf{k}_{\phi}\sin\nu_{\phi}. \tag{8}$$

We recall that ν is the angle of the propagating wave and k the modulus of the corresponding wave vector $\mathbf{k}$, as shown in Fig. 1. The latter wave vector is scaled with the mean speed of sound, $\overline{c}$, and the angular frequency to yield the dimensionless wave vector, $\mathbf{K}=\mathbf{k}\overline{c}/\omega$. According to Marble and Candel [31] the frequency and the tangential component of the wave vector k_y are conserved for the wave propagation through the turbine stages. This component is also related to the azimuthal mode

order m through $k_{\phi,y} = m/R$. Yet, this is not the case for the dimensionless tangential component $K_{\phi,y}$, since the mean speed of sound may vary through the blade rows.

Eqs. (1)–(4) can then be used to relate, for each wave, the wave vector to the angular frequency, the mean Mach number $\overline{M} = \overline{w}/\overline{c}$, and the flow direction $\overline{\theta}$.

2.1.1. Entropy wave

The entropy wave, $w^s = s'/C_p$, is defined as

$$w^s = \frac{s'}{C_p} = A_s \exp\left[-\mathrm{i}(\omega t - \mathbf{k}_s \cdot \mathbf{x})\right]. \tag{9}$$

The dispersion equation is obtained by combining Eq. (9) with the transport equation of the entropy wave, Eq. (4),

$$K_s \overline{M} \cos\left(\nu_s - \overline{\theta}\right) - 1 = 0. \tag{10}$$

This dispersion equation then yields the axial component of the wave vector, $K_{s,x}$, as a function of the tangential component, the angular frequency, and the mean flow Mach number and direction.

By definition, the entropy wave does not yield pressure or velocity perturbations, and the fluctuations of the primitive variables (s'/Cp, $w'/\overline{c}$, $p'/\gamma\overline{p}$ and θ') generated by the entropy wave are therefore

$$\begin{Bmatrix} s'/C_p \\ w'/\overline{c} \\ p'/\gamma\overline{p} \\ \theta' \end{Bmatrix}_s = \begin{Bmatrix} 1 \\ 0 \\ 0 \\ 0 \end{Bmatrix} w^s. \tag{11}$$

2.1.2. Vorticity wave

The vorticity wave is defined as the curl of the fluctuating velocity field

$$\xi' = \frac{\partial v'}{\partial x} - \frac{\partial u'}{\partial y}. \tag{12}$$

The transport equation for the vorticity wave can be derived from Eqs. (2) and (3). Differentiating Eq. (2) with respect to y and Eq. (3) with respect to x lead to

$$\begin{aligned} \frac{\partial}{\partial y}\left(\frac{\mathrm{D}}{\mathrm{D}t}(u')\right) &= -\frac{1}{\overline{\rho}}\frac{\partial^2 p'}{\partial x \partial y}, \\ \frac{\partial}{\partial x}\left(\frac{\mathrm{D}}{\mathrm{D}t}(v')\right) &= -\frac{1}{\overline{\rho}}\frac{\partial^2 p'}{\partial y \partial x}. \end{aligned} \tag{13}$$

Subtracting both relations and using Schwarz's theorem, the pressure term can be eliminated, yielding the vorticity equation

$$\frac{\mathrm{D}}{\mathrm{D}t}(\xi') = 0. \tag{14}$$

As the entropy wave, the vorticity wave can be assumed harmonic and monochromatic,

$$w^v = \frac{\xi'}{\omega} = A_v \exp\left[-\mathrm{i}(\omega t - \mathbf{k}_v \cdot \mathbf{x})\right]. \tag{15}$$

The dispersion equation of the vorticity wave can be obtained by combining Eq. (14) with Eq. (15), namely

$$K_v \overline{M} \cos\left(\nu_v - \overline{\theta}\right) - 1 = 0. \tag{16}$$

As shown by Chu and Kovasznay [7], no pressure or entropy fluctuations are associated with this wave to first order. Eq. (4) then shows that there are no density fluctuations either. Eq. (1) can be reduced to

$$\frac{\partial u'}{\partial x} + \frac{\partial v'}{\partial y} = 0. \tag{17}$$

Using Eq. (15) the velocity field can be written as

$$\begin{aligned} \frac{u'}{\overline{c}} &= -\mathrm{i}\frac{\xi'}{\omega}\frac{\sin(\nu_v)}{K_v}, \\ \frac{v'}{\overline{c}} &= \mathrm{i}\frac{\xi'}{\omega}\frac{\cos(\nu_v)}{K_v}. \end{aligned} \tag{18}$$

These fluctuations are recast in terms of w' and θ' using Eq. (6)

$$\frac{w'}{\overline{c}} = -\mathrm{i}\frac{\xi'}{\omega}\frac{\sin\left(\nu_v - \overline{\theta}\right)}{K_v},$$

$$\theta' = \mathrm{i}\frac{\xi'}{\omega}\frac{\cos\left(\nu_v-\overline{\theta}\right)}{\overline{M}K_v}. \tag{19}$$

Using the dimensionless form of the vorticity wave, $w^v=\xi'/\omega$, the fluctuations of the primitive variables generated by this wave are

$$\begin{Bmatrix} s'/C_p \\ w'/\overline{c} \\ p'/\gamma\overline{p} \\ \theta' \end{Bmatrix}_v = \begin{Bmatrix} 0 \\ -\mathrm{i}\dfrac{\sin\left(\nu_v-\overline{\theta}\right)}{K_v} \\ 0 \\ \mathrm{i}\dfrac{\cos\left(\nu_v-\overline{\theta}\right)}{\overline{M}K_v} \end{Bmatrix} w^v. \tag{20}$$

2.1.3. Acoustic waves

A transport equation for the pressure fluctuations can be obtained by combining Eqs. (1)–(4). Eq. (4) is first used to eliminate the density term in Eq. (1) and a substantial derivative of the resulting equation is taken,

$$\left[\left(\frac{\mathrm{D}}{\mathrm{D}t}\right)^2\right]\left(\frac{p'}{\gamma\overline{p}}\right)+\frac{\mathrm{D}}{\mathrm{D}t}\left(\frac{\partial u'}{\partial x}\right)+\frac{\mathrm{D}}{\mathrm{D}t}\left(\frac{\partial v'}{\partial y}\right)=0. \tag{21}$$

Combining Eq. (21) with the substantial derivative of Eqs. (2) and (3), and knowing that $\overline{c}^2=\gamma\overline{p}/\overline{\rho}$ yields the following equation for the pressure perturbations:

$$\left[\left(\frac{\mathrm{D}}{\mathrm{D}t}\right)^2-\overline{c}^2\left(\frac{\partial^2}{\partial x^2}+\frac{\partial^2}{\partial y^2}\right)\right]\left(\frac{p'}{\gamma\overline{p}}\right)=0. \tag{22}$$

Using the waveform of Eq. (7) for the acoustic waves,

$$w^{\pm}=\left(\frac{\rho'}{\gamma\overline{\rho}}\right)_{\pm}=A_{\pm}\exp\left[-\mathrm{i}(\omega t-\mathbf{k}_{\pm}\cdot\mathbf{x})\right], \tag{23}$$

the following dispersion equation is obtained:

$$\left(1-K_{\pm}\overline{M}\cos\left(\nu_{\pm}-\overline{\theta}\right)\right)^2-K_{\pm}^2=0, \tag{24}$$

where $K_{\pm}$ is the module of the dimensionless wave vector. As the above acoustic dispersion equation, Eq. (24) has two solutions, the subscript $(\pm)$ stands for the acoustic perturbations propagating downstream $(+$, called the transmitted acoustic wave) and upstream $(-$, called the reflected acoustic wave). This dispersion equation can be rewritten as a function of the axial and tangential components ($K_{\pm,x}$ and $K_{\pm,y}$) using Eq. (8),

$$\left(1-K_{\pm,x}\overline{M}\cos\overline{\theta}-K_{\pm,y}\overline{M}\sin\overline{\theta}\right)^2-K_{\pm,x}^2-K_{\pm,y}^2=0. \tag{25}$$

When solving for $K_{\pm,x}$ in Eq. (25), $K_{\pm,x}$ can be either a real or a complex value. The real values correspond to acoustic waves propagating without attenuation through the mean steady flow (cut-on modes), while complex values are evanescent waves that cannot propagate in the flow (cut-off modes). Solving for cut-on modes in Eq. (25) yields the condition

$$\left(1-K_{\pm,y}\overline{M}\sin\overline{\theta}\right)^2-\left(1-\overline{M}^2\sin^2\overline{\theta}\right)K_{\pm,y}^2<0. \tag{26}$$

For a given mean flow, this relationship, Eq. (26), gives a critical value $K_{\pm,y}=\overline{c}k_{\pm,y}/\omega$. This shows that for any tangential acoustic mode $k_{\pm,y}$ there exists a cut-off frequency below which the acoustic waves do not propagate.

Knowing that the wave is isentropic and irrotational [7], the fluctuations of primitive variables generated by the acoustic waves can then be obtained,

$$\begin{Bmatrix} s'/C_p \\ w'/\overline{c} \\ p'/\gamma\overline{p} \\ \theta' \end{Bmatrix}_{\pm} = \begin{Bmatrix} 0 \\ K_{\pm}\cos\left(\nu_{\pm}-\overline{\theta}\right)/[1-K_{\pm}\overline{M}\cos\left(\nu_{\pm}-\overline{\theta}\right)] \\ 1 \\ K_{\pm}\sin\left(\nu_{\pm}-\overline{\theta}\right)/[\overline{M}(1-K_{\pm}\overline{M}\cos\left(\nu_{\pm}-\overline{\theta}\right))] \end{Bmatrix} w^{\pm}. \tag{27}$$

2.1.4. Transformation matrix

Finally, the primitive fluctuating variables can be recast in a matrix form by adding the contribution of each of the four waves, leading to the following vector relationship:

$$\begin{Bmatrix} s'/C_p \\ w'/\overline{c} \\ p'/\gamma\overline{p} \\ \theta' \end{Bmatrix} = [\mathbf{M}] \cdot \begin{Bmatrix} w^s \\ w^v \\ w^+ \\ w^- \end{Bmatrix}, \tag{28}$$

where the matrix [**M**] is given by the combination of Eqs. (11), (20) and (27),

$$[\mathbf{M}] = \begin{bmatrix} 1 & 0 & 0 & 0 \\ 0 & -\mathrm{i}\frac{\sin(\nu_v-\overline{\theta})}{K_v} & \frac{K_+\cos(\nu_+-\overline{\theta})}{\left(1-K_+\overline{M}\cos(\nu_+-\overline{\theta})\right)} & \frac{K_-\cos(\nu_--\overline{\theta})}{\left(1-K_-\overline{M}\cos(\nu_--\overline{\theta})\right)} \\ 0 & 0 & 1 & 1 \\ 0 & \mathrm{i}\frac{\cos(\nu_v-\overline{\theta})}{K_v\overline{M}} & \frac{K_+\sin(\nu_+-\overline{\theta})}{\overline{M}\left(1-K_+\overline{M}\cos(\nu_+-\overline{\theta})\right)} & \frac{K_-\sin(\nu_--\overline{\theta})}{\overline{M}\left(1-K_-\overline{M}\cos(\nu_--\overline{\theta})\right)} \end{bmatrix}. \tag{29}$$

2.2. Jump conditions through the blade row

Once the primitive variables are related to the acoustic, entropy and vorticity waves by Eq. (29) in both upstream and downstream regions of a blade or vane row, only a relationship between the primitive variables on both sides is needed to close the problem. Since each blade or vane row is assumed axially compact, the upstream and downstream flow relationship reduces to a jump condition at the interface. Eq. (28) shows that four conditions are required. The latter are obtained using the conservation of mass and energy, and the transport of entropy fluctuations, plus a fourth equation on the tangential component of the flow, obtained through the so-called Kutta condition. As a different form of energy is conserved through stationary and rotating rows, the study of the stator vane and of the rotor blade are done separately.

2.2.1. Stator vane

For the stator vane, the conservation equations of mass and stagnation enthalpy or equivalently stagnation temperature, and the transport of entropy fluctuations, used by Cumpsty and Marble [9] read,

$$\begin{aligned} \left(\frac{\dot{m}'}{\overline{\dot{m}}}\right)_1 &= \left(\frac{\dot{m}'}{\overline{\dot{m}}}\right)_2, \\ \left(\frac{T_t'}{\overline{T_t}}\right)_1 &= \left(\frac{T_t'}{\overline{T_t}}\right)_2, \\ \left(\frac{s'}{C_p}\right)_1 &= \left(\frac{s'}{C_p}\right)_2. \end{aligned} \tag{30}$$

Subscripts 1 and 2 stand for the flow upstream and downstream of the vane row, as shown in Fig. 1. These equations should be rewritten as a function of the primitive variables used previously (s', p', w' and θ'). For the mass and temperature fluctuations, it yields

$$\left(\frac{\dot{m}'}{\overline{\dot{m}}}\right) = \frac{p'}{\gamma\overline{p}} + \frac{1}{\overline{M}}\frac{w'}{\overline{c}} - \theta'\tan\overline{\theta}, \tag{31}$$

$$\left(\frac{T_t'}{T_t}\right) = \frac{1}{1+\frac{(\gamma-1)}{2}\overline{M}^2}\left[(\gamma-1)\frac{p'}{\gamma\overline{p}} + \frac{s'}{C_p} + (\gamma-1)\overline{M}\frac{w'}{\overline{c}}\right]. \tag{32}$$

As mentioned above, Eqs. (30)–(32) should be completed by a fourth condition: Cumpsty and Marble [9] applied the Kutta condition at the vane outlet. The potential-flow theory indicates that in a steady flow around an airfoil, the effect of viscosity can be accounting for by imposing a condition which removes the trailing-edge pressure or velocity singularity. This condition fixes the pressure jump or the circulation around the airfoil such that the stagnation point is located at the trailing-edge. For unsteady flows, the Kutta condition used by Cumpsty and Marble [9] states that the flow deviation θ_2 is equal to the geometrical angle of the vane trailing edge, and therefore its perturbation should be zero ($\theta_2' = 0$). Imposing the correct condition at the trailing edge of the vane row is important to correctly predict the generation of noise at the vane trailing edge and, in our case, the acoustic transfer functions of the stator vane. Cumpsty and Marble [9] suggest to use a more general unsteady form of the Kutta condition given by

$$\theta_2' = \beta\theta_1', \tag{33}$$

where β is either measured when experimental data are available or calculated by semi-empirical methods. In the low-frequency limit used in the present analysis, the Kutta condition with $\beta = 0$ is generally valid as the flow evolves quasi-steadily.

Consequently, the jump conditions are obtained by rewriting Eqs. (30) and (33) in a matrix form as a function of the primitive variables, which read

$$[\mathbf{E}_1]\cdot\begin{Bmatrix} s'/C_p \\ w'/\overline{c} \\ p'/\gamma\overline{p} \\ \theta' \end{Bmatrix}_1 = [\mathbf{E}_2]\cdot\begin{Bmatrix} s'/C_p \\ w'/\overline{c} \\ p'/\gamma\overline{p} \\ \theta' \end{Bmatrix}_2, \tag{34}$$

where $[\mathbf{E}_1]$ and $[\mathbf{E}_2]$ are defined as

$$[\mathbf{E}_1] = \begin{bmatrix} 1 & 0 & 0 & 0 \\ -1 & \frac{1}{\overline{M}_1} & 1 & -\tan\overline{\theta}_1 \\ \frac{\mu_1}{\gamma-1} & \mu_1\overline{M}_1 & \mu_1 & 0 \\ 0 & 0 & 0 & \beta \end{bmatrix},$$

$$[\mathbf{E}_2] = \begin{bmatrix} 1 & 0 & 0 & 0 \\ -1 & \frac{1}{\overline{M}_2} & 1 & -\tan\overline{\theta}_2 \\ \frac{\mu_2}{\gamma-1} & \mu_2\overline{M}_2 & \mu_2 & 0 \\ 0 & 0 & 0 & 1 \end{bmatrix}, \tag{35}$$

and $\mu = 1/[1+(\gamma-1)\overline{M}^2/2]$.

2.2.2. Rotor blade

For a rotor blade, the conservation of stagnation enthalpy (Section 2.2.1) is no longer valid. Instead, the conserved variable through the blade row is the rothalpy defined as [5,30],

$$I = h_t - U\overline{v}, \tag{36}$$

where h_t is the specific stagnation enthalpy, U the rotating speed of the blade, and $\overline{v}$ the tangential component of the absolute speed (Fig. 2). For the rotating speed, different values are considered at the inlet and outlet of the blade row to account for the large expansion of the turbine. The conservation of rothalpy can be derived by combining the energy equation and Euler's equation, and reads

$$\Delta h_t = \Delta(Uv) = U_2\cdot v_2 - U_1\cdot v_1. \tag{37}$$

Considering small perturbations, a generalized form of the energy equation for rotating blades can then be deduced as,

$$\frac{I_1'}{\overline{I}_1} = \frac{I_2'}{\overline{I}_2}, \tag{38}$$

which replaces the second equation in Eq. (30) for the stagnation temperature jump. The rothalpy fluctuation is then written

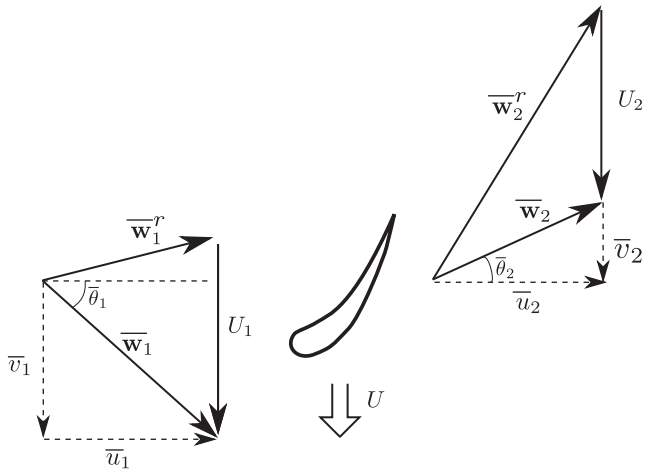

Fig. 2. Sketch of the flow through a rotor blade. Superscript $()^r$ represents the variables in the rotor reference frame.

as a function of the primitive variables,

$$\frac{I'}{\overline{I}}=\frac{h_t'-Uv'}{\overline{h_t}-U\overline{v}}=\frac{\dfrac{h_t'}{\overline{h_t}}-\dfrac{U\overline{v}}{\overline{h_t}}\dfrac{v'}{\overline{v}}}{1-\dfrac{U\overline{v}}{\overline{h_t}}}. \tag{39}$$

Knowing that $h_t=C_pT_t$ and defining the parameter ζ as

$$\zeta=\frac{U\overline{v}}{\overline{h_t}}, \tag{40}$$

Eq. (39) can be recast into,

$$\frac{I'}{\overline{I}}=\frac{1}{1-\zeta}\left[\frac{T_t'}{\overline{T_t}}-\zeta\left(\frac{v'}{v}\right)\right]. \tag{41}$$

As expected, $U=0$ implies that $\zeta=0$ (Eq. (40), thus the stagnation temperature jump used for the stator vane is recovered. Moreover, the fluctuating tangential velocity v'/v can be eliminated using Eqs. (6), and (41)) becomes

$$\frac{I'}{\overline{I}}=\frac{1}{1-\zeta}\left[\frac{T_t'}{\overline{T_t}}-\zeta\left(\frac{1}{\overline{M}}\frac{w'}{\overline{c}}+\frac{\theta'}{\tan\overline{\theta}}\right)\right], \tag{42}$$

which replaces the stagnation enthalpy conservation in Eqs. (34) and (35). For a rotor, the Kutta condition has to be imposed in its reference frame, yielding

$$(\theta')_2^r=\beta(\theta')_1^r, \tag{43}$$

where $(\theta')^r$ is the fluctuation of the relative flow angle. This equation can be recast in the fixed reference frame using the variables θ' and $w'/\overline{w}$ (Fig. 2) and trigonometric relations (Appendix A) as follows:

$$(\theta')^r=\theta'\left(1+\frac{U}{\overline{w^r}}\sin\left(\overline{\theta^r}\right)\right)+\left(\frac{w'}{\overline{w}}\right)\frac{U}{\overline{w^r}}\cos\left(\overline{\theta^r}\right). \tag{44}$$

2.3. Solution of the propagation equations through a compact multi-stage turbomachinery

The propagation equations through a compact multi-stage turbomachinery are solved in a matrix form by imposing the correct waves and boundary conditions at each rotating or stationary row. In the subsonic case, the latter are w^+, w^s and w^v at the inlet, and w^- at the outlet of the blade or vane row. For instance the waves coming from the combustion chamber must be first decomposed into azimuthal modes related to k_y, and into angular frequencies ω. The propagation equations are solved for each pair $(k_y,\ \omega)$ for which the proper dispersion equations can be used to obtain the value of the complete dimensionless wave vector $\mathbf{K}$ on both sides of a blade or vane row for each wave. Using this information, matrices $\mathbf{M}$ and $\mathbf{E}$ can then be computed on both sides of the blade or vane row.

For a single row, the problem is solved by writing Eq. (34) as a function of the waves using Eq. (28),

$$\underbrace{[\mathbf{E}_1]\cdot[\mathbf{M}_1]}_{[\mathbf{B}_1]}\cdot\left\{\begin{array}{c}w^s\\w^v\\w^+\\w^-\end{array}\right\}_1=\underbrace{[\mathbf{E}_2]\cdot[\mathbf{M}_2]}_{[\mathbf{B}_2]}\cdot\left\{\begin{array}{c}w^s\\w^v\\w^+\\w^-\end{array}\right\}_2. \tag{45}$$

The boundary conditions for each row should only provide the incoming waves. Therefore, Eq. (45) is recast into "scattering matrices" $[\mathbf{A}_{\text{in}}]$ and $[\mathbf{A}_{\text{out}}]$ by permuting the fourth column of matrices $[\mathbf{B}_1]$ and $[\mathbf{B}_2]$ and changing signs. Such a matrix transformation allows the construction of an equivalent system with imposed waves on the right-hand side of the equations, and the unknowns on the left-hand side only. The "scattered" system replacing Eq. (45) can then be inverted to yield the unknown out-coming waves, and reads

$$[\mathbf{A}_{\text{out}}]\cdot\left\{\begin{array}{c}w_2^s\\w_2^v\\w_2^+\\w_1^-\end{array}\right\}=[\mathbf{A}_{\text{in}}]\cdot\left\{\begin{array}{c}w_1^s\\w_1^v\\w_1^+\\w_2^-\end{array}\right\}. \tag{46}$$

For the case of multiple blade and vane rows of a typical turbomachinery, a phase-shift of the waves through the row spacing is applied to account for the wave propagation through the entire machine and the interstage gaps. Indeed, even if each stator vane or rotor blade can be assumed compact (at least for sufficiently low frequencies), the whole multi-stage turbine is not, because of a cumulative effect. The complete phase shift is therefore recovered by adding a phase shift to each component, based on an equivalent axial length L. In this study, this length is chosen as the interstage gap corrected with half the chord length of adjacent components, namely $L=L_{\mathbf{stator}}/2+L_{\mathbf{interstage}}+L_{\mathbf{rotor}}/2$. Since no wave coupling occurs for

pure wave propagation, a diagonal matrix [**T**] is used to impose the phase-shift of the waves, which reads

$$[\mathbf{T}] = \begin{bmatrix} \exp(\mathrm{i}k_x^s L) & 0 & 0 & 0 \\ 0 & \exp(\mathrm{i}k_x^v L) & 0 & 0 \\ 0 & & \exp(\mathrm{i}k_x^+ L) & 0 \\ 0 & 0 & 0 & \exp(\mathrm{i}k_x^- L) \end{bmatrix}, \tag{47}$$

Considering $\mathbf{V}_u^i$ and $\mathbf{V}_d^i$ the wave vectors upstream and downstream of the i-th blade or vane row respectively, Eq. (45) connects both sides through

$$\left[\mathbf{B}_1^i\right] \cdot \mathbf{V}_u^i = \left[\mathbf{B}_2^i\right] \cdot \mathbf{V}_d^i. \tag{48}$$

The downstream wave vector can be related to the following blade or vane row by $\mathbf{V}_u^{i+1} = [\mathbf{T}^i] \cdot \mathbf{V}_d^i$. Combining the successive stages of a turbine, a relationship between the inlet and the outlet waves of the whole turbomachine can be written in a matrix form,

$$\left[\prod_{i=1}^{N_r-1} \left\{ \left[\mathbf{B}_1^{i+1}\right] \mathbf{T}^i \left[\mathbf{B}_2^i\right]^{-1} \right\}\right] \left[\mathbf{B}_1^1\right] \cdot \mathbf{V}_u^1 = \left[\mathbf{B}_2^{N_r}\right] \cdot \mathbf{V}_d^{N_r}, \tag{49}$$

where N_r is the number of rows. This system of equations can be finally permuted to obtain a "scattered" system similar to Eq. (46), which can be inverted to provide the unknown out-coming waves. The resulting analytical tool has been termed CHORUS and included for instance in a complete methodology for predicting combustion noise termed CONOCHAIN [29].

Even though the combination of several blade and vane rows leads to a transfer function which is frequency dependent through the wave propagation modeled by Eq. (47), the compact assumption for each individual row still limits the present model to the low frequency range.

Finally note that when the parameter of the Kutta condition β is equal to zero, the system of equations becomes singular and can no longer be inverted. In practice this singular condition is avoided by using a small value, $\beta = 10^{-9}$.

3. Numerical simulations

The goal of the numerical simulations is to obtain realistic transfer functions of a turbine stage in order to compare them with the analytical method predictions, and evaluate the range of validity of the theoretical model described in Section 2. The case of a single stator vane was already studied in detail by Leyko et al. [24,23], and that of a rotor blade by Wang et al. [43]. Thus, this section focuses on a stator–rotor stage configuration, where the extension of the theory to rotating blades is again analyzed, and the effect of successive turbine rows is unraveled. Such a simulation involves a very large range of characteristic time scales: on the one hand, the small details of the turbulent flow should be resolved or modeled; on the other hand the frequency of the acoustic and entropy perturbations remains large because of the compact assumption. For this reason, the analysis is performed in a 2D stator–rotor configuration as shown in Fig. 3. This has two main implications: first, the flow is considered two-dimensional and therefore no realistic turbulent mixing is computed as the large vortical structures generated at the blade or vane trailing edge cannot develop into fine three-dimensional turbulence. Second, only longitudinal plane waves with no tangential component can be studied as the computation is limited to a single stator vane–rotor blade using periodic boundary conditions.

The 2D compressible flow in the turbine stage is computed with AVBP the reactive Large-Eddy-Simulation (LES) code jointly developed by Cerfacs and IFP-EN [2,37,8]. The Smagorinsky sub-grid-scale model is used for stability purpose and not to model turbulence. The laminar and turbulent Prandtl numbers are kept large to reduce heat diffusion and isolate this effect from the transmission problem addressed here. All simulations are performed with the TTG4A numerical scheme which is third order in space and fourth order in time [10].

To compute the relative displacement of the rotor, the MISCOG methodology is applied [43], in which the stator and rotor are simulated separately in two different simulations, and coupled at the interface through an interpolation on an overlapped region (Fig. 4). The number of nodes in the overlapping region must verify a stability criteria, which depends on the

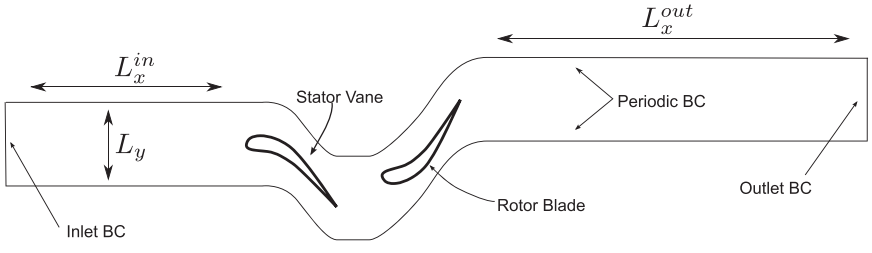

Fig. 3. Sketch of the computational domain.

order of the discretization scheme, as explained by Wang et al. [43]. This method has been shown to propagate correctly both acoustic and hydrodynamic perturbations through the interface with little dissipation, dispersion, or numerical errors. In the preliminary study [12], this coupling method was shown to yield similar or smoother transfer functions as the classical ALE method. Longer computational time has been also achieved compared with [12], which yields more accurate results at low frequencies.

3.1. Boundary conditions and forcing term

Fig. 3 shows the boundary conditions imposed in the present configuration. Periodicity is first imposed at the top and bottom boundaries to account for the actual cascade. A no-slip boundary condition in the proper reference frame is applied on the stator and rotor walls, with a wall-model to impose the wall shear stress (high-Reynolds approach). The Navier–Stokes Characteristic Boundary Condition (NSCBC) method developed by Poinsot and Lele [36] is used at both inlet and outlet to impose the wave forcing and to avoid the reflection of acoustic waves.

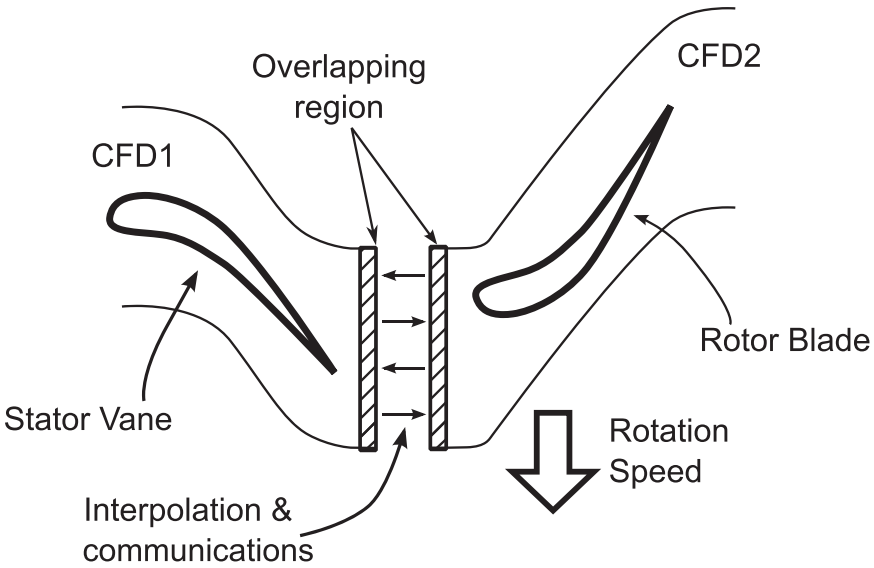

Fig. 4. Sketch of the interface between the two simulations: CFD1 and CFD2.

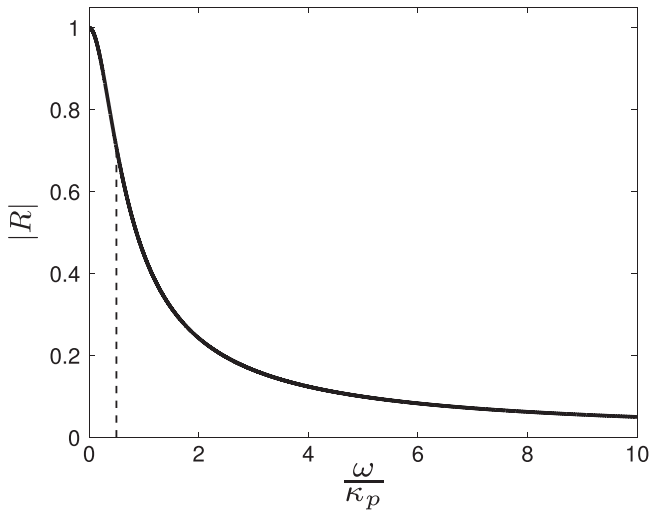

Fig. 5. Reflecting coefficient (—) of the outlet boundary condition. – – –: cutoff angular frequency $\omega/\kappa_p = 0.5$, leading to $|R_{\mathbf{out}}| = 1/\sqrt{2}$ (-3 **dB**). Below this limit, $\omega/\kappa_p < 0.5$, the boundary condition can be considered as fully reflecting.

At the outlet, the mean pressure is imposed by the following NSCBC:

$$\frac{\partial w^-}{\partial t} - L^- = 0, \tag{50}$$

where w^- stands for the acoustic wave entering the domain. L^- cannot be set to exactly zero, e.g. a perfectly non-reflecting boundary condition, because the mean pressure is no longer imposed, leading to a pressure drift. Consequently, a relaxed formulation is preferred, writing L^- as a function of the difference between the local pressure p and the target one p_{ref}, multiplied by a relaxation parameter κ_p:

$$L^- = \kappa_p (p - p_{\text{ref}}) / (\gamma p_{\text{ref}}). \tag{51}$$

Large values of κ_p impose a reflecting boundary condition whereas low values a non-reflecting one. Selle et al. [38] showed that such a boundary condition is equivalent to a first-order low-pass filter,

$$R_{\text{out}} = \frac{-1}{1 - 2i\omega/\kappa_p}. \tag{52}$$

Fig. 5 shows the reflecting coefficient, showing that for $\omega/\kappa_p > 10$, the reflected wave is smaller than 5 percent of the incident wave. In practice, a modification of the NSCBC proposed by Yoo et al. [44] is implemented to ensure that vortices generated by the blunt trailing edge of the blade or vane (see below in Section 4) are convected throughout the outlet boundary without producing spurious noise.

The inlet boundary condition is treated in the same way, but with a relaxed formulation based on the velocity for the downstream acoustic wave w^+, and on the temperature for the entropy wave w^s [12]. The inlet reflecting coefficient can be shown to have the same behavior as the outlet boundary condition.

To compute the acoustic and entropy transfer functions of the complete turbine stage, acoustic or entropy waves are injected into the LES domain through the inlet NSCBC, starting from a statistically converged mean flow through the blade rows. The injected wave is composed of multiple components spaced by 100 Hz, to compute several frequencies in a single simulation. Consequently, the forced wave reads

$$w_f = A^f f(t), \quad \text{with } f(t) = \sum_{n=1}^{N} \sin(2\pi n f_0 t), \tag{53}$$

where A^f is a sufficiently small amplitude to ensure a linear acoustic response. The function $f(t)$ is composed of $N = 50$ frequencies (Fig. 6), with the fundamental frequency $f_0 = 100$ Hz. It should be noted that Duran also tested a random phase-shift added to the function $f(t)$ but it yielded similar results [11]. Yet, it allowed larger amplitudes of the forced waves without causing a nonlinear response. To impose this forcing term in the NSCBC, the term L^+ is modified to add the contribution of the forcing wave,

$$L^f = \frac{\kappa_f}{c_{\text{ref}}} (\Psi - \Psi_{\text{ref}} - \Psi_f) + \frac{\partial w_f}{\partial t}, \tag{54}$$

where the term w_f is the acoustic or entropy forced wave, Ψ is the primitive variable associated with the wave type to describe the NSCBC inlet condition (i.e. $\Psi = u$ for the acoustic wave, and $\Psi = T$ for the entropy wave), Ψ_f is the primitive fluctuation caused by the forcing w_f, and c_{ref} is a normalization constant. For forced simulations, the relaxation coefficient of the NSCBC is set to $\kappa_f = 10\ \text{s}^{-1}$, again ensuring no drift of the mean flow variable Ψ while minimizing the reflection of waves.

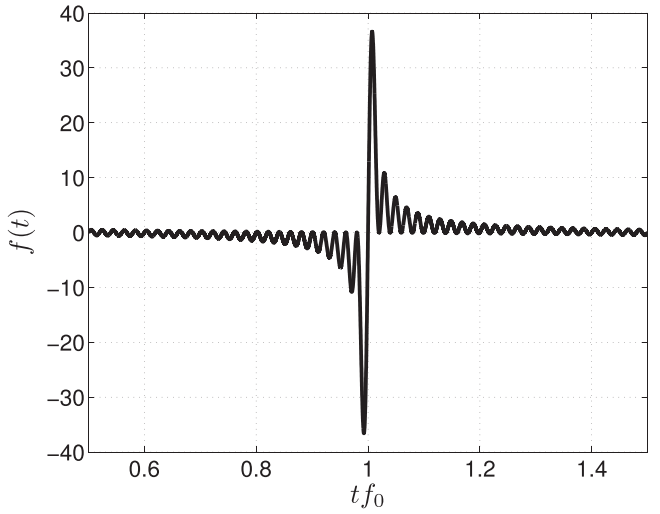

Fig. 6. Function $f(t)$ used to pulse the boundary conditions plotted with $N = 50$.

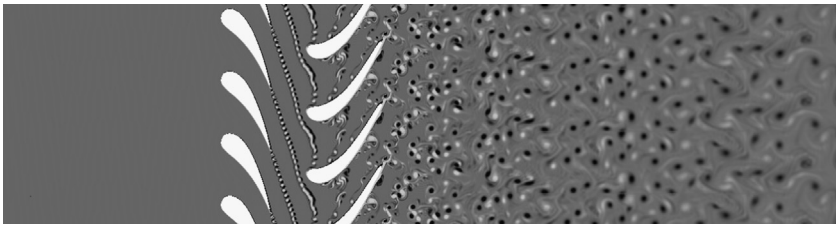

Fig. 7. Vorticity field of the flow.

To ensure the statistical convergence of the results, the simulations are run for at least 65 periods of the lowest frequency, discarding the first five associated with transient phenomenon, and using the other 60 or more periods for the post-processing. This is quite similar to what was used in the stator vane by Leyko et al. [23].

3.2. Post-processing of the waves

Even though no turbulence is injected at the inlet, the no-slip condition at the stator and rotor blades generate a trailing-edge vortex-shedding. Fig. 7 reveals the 2D vorticity field at an instant prior to the injection of waves through the boundary condition. These eddies cannot develop properly into small scale turbulence (vortex stretching in the spanwise direction) because of the 2D configuration, but their presence perturbs the entropy and acoustic waves. For this reason the wave post-processing is performed in the full inlet and outlet regions to calculate the transmitted and reflected waves for each simulation. The post-processing is then performed in 5 steps, as proposed by Leyko et al. [24] for the single stator case:

1. *Steady-state calculation*: The mean flow variables are computed at the inlet and outlet.
2. *Wave calculation*: Primitive variables (s'/C_p, $w'/\overline{c}$, $p'/\gamma\overline{p}$ and θ') are calculated at each point as a function of time. Using the matrix [**M**] given in Eq. (29), the four waves w^s, w^v, w^+, w^- are calculated as a function of x, y and t, in both the inlet and outlet regions.
3. *Integration along the transverse direction*: These waves are averaged along the transverse direction, since only plane waves are considered in this study. For a wave type ϕ,

$$w_x^{\phi}(x,t) = \frac{1}{L_y}\int_0^{L_y} w^{\phi}(x,y,t)\,\mathrm{d}y. \tag{55}$$

4. *Fourier-Transform*: The Fourier-Transform is performed at the discrete frequencies considered in Eq. (53)

$$w_x^{\phi}(x,k) = \left|\frac{1}{t_f}\int_0^{t_f} w_x^{\phi}(x,t)\exp(2\pi i f_0 k t)\,\mathrm{d}t\right|. \tag{56}$$

5. *Integration along the propagating direction*: The Fourier transform is finally integrated along the x-axis to average the solution,

$$w^{\phi}(k) = \sqrt{\frac{1}{L_x}\int_0^{L_x}\left[w_x^{\phi}(x,k)\right]^2\,\mathrm{d}x}. \tag{57}$$

4. Results

The mean flow characteristics are given in Table 1. Using these mean flow variables, the analytical model described in Section 2 is used to compute the acoustic and entropy transfer functions of the turbine stage. The acoustic reflection and transmission coefficients are plotted in Fig. 8, comparing the analytical method with the numerical simulations of the stator–rotor stage. As previously mentioned, even if the analytical theory is frequency-dependent, the method is still based on the compact assumption and therefore is strictly valid only for low frequencies. Yet, noticeably, the method performs well for frequencies ranging from 0 to 2000 Hz, and even up to 4000 Hz in the case of the transmitted wave. The value of the reduced frequency $\Omega = fl_x/c$ obtained using the stator axial length l_x is also plotted. The analytical method is seen to predict the transmitted and reflected acoustic waves within reasonable accuracy for at least $\Omega < 0.1$.

Similar results are obtained for the entropy transfer functions dedicated to indirect combustion noise (Fig. 9). The analytical method and the numerical simulations are again seen to agree for the low frequency range (i.e. $\Omega < 0.1$), where the compact assumption holds.

However, for higher frequencies (i.e. $\Omega > 0.1$), large discrepancies appear between the numerical and the analytical transfer functions. Both the reflected and transmitted coefficients computed numerically by LES tend to zero (● in Fig. 9), while the analytical method does not (— in Fig. 9). This is due to the assumption made in the analytical method of Section 2, which considers that the entropy wave is propagated unaltered through the stator and rotor blades. Fig. 10 reveals that the

Table 1
Mean flow characteristics, where the compression ratio is defined as $\Pi = P_{i2}/P_{i1}$, and the load factor corresponds to $\psi = -\Delta h_t/U^2$.

Mean flow characteristics	STATOR		ROTOR	
	Inlet	Outlet	Inlet	Outlet
Mach	0.166	0.661	0.661	0.31
θ	0	−71.8	−71.8	−32.7
$\bar{c}$ (m/s)	798.3	773.0	773.0	755.1
γ	0.13	0.13	0.13	0.13
U (m/s)	0		−500	
Π	1		0.67	
ψ	0		0.75	

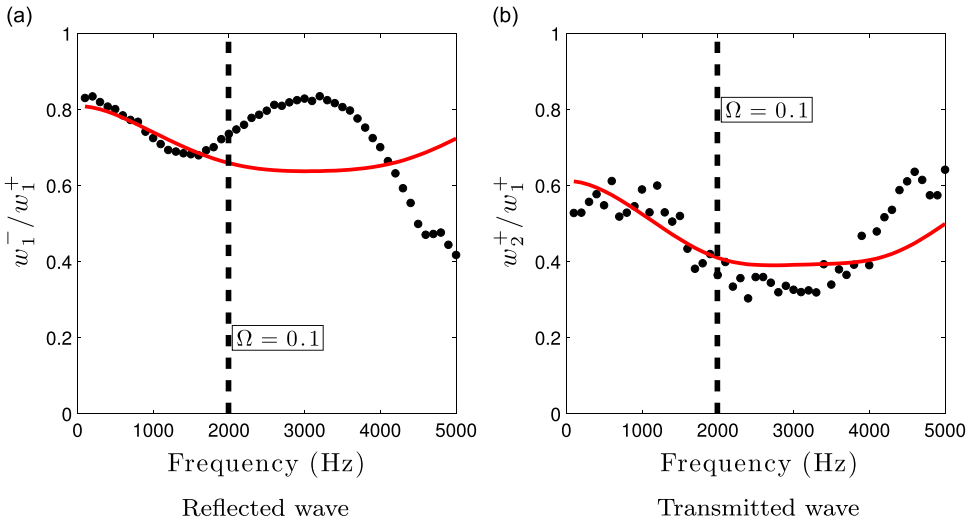

Fig. 8. Acoustic transfer functions. —: Analytical theory ; ○: Numerical simulations.

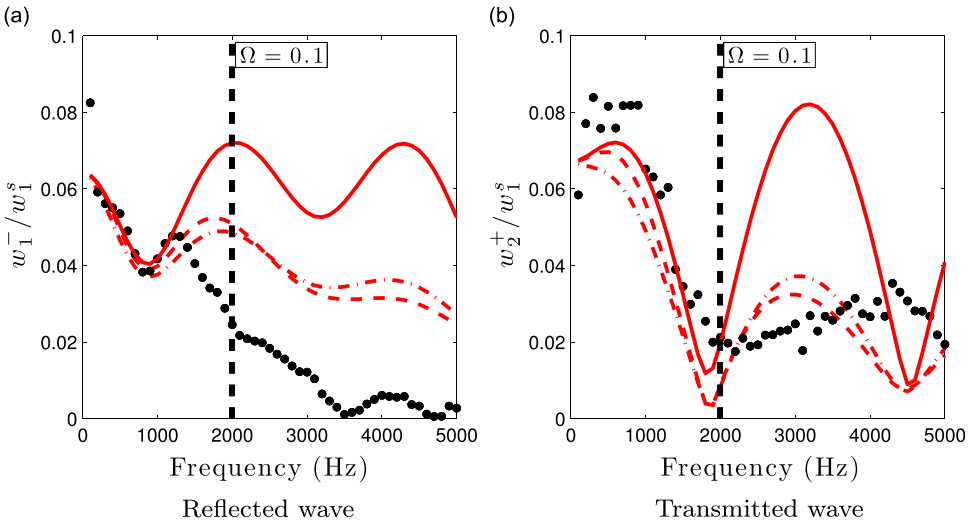

Fig. 9. Entropy transfer functions. —: Analytical theory without attenuation ; – – –: Analytical theory with attenuation extracted from the simulation ; – · – · : Analytical theory with a simplified attenuation model ; ●: Numerical simulations.

entropy spot is not conserved through the stages. This was already observed by Leyko et al. [23] for the case of a single stator blade. The initial planar entropy waves are distorted by the 2D mean flow. Indeed, the potential flow induced by the thick blade under an incident flow, combined with the no-slip conditions on the stator and rotor blades, imposes an azimuthal dependency (y) of the mean flow, which has been neglected in the analytical model. This 2D flow prescribes a propagating velocity to the entropy wave which is dependent on the azimuthal direction, deforming the initial planar front at the length-scale of the pitch length, l_y. It is worth noting that the total entropy fluctuation is not dissipated, but re-distributed in higher-order propagating modes. Actual entropy dissipation caused by turbulent mixing may also exist in the simulation, but is not accounted for in the theoretical analysis performed here, since it requires a realistic 3D simulation.

Leyko et al. [23] used the mean flow through the stator blade to predict the decrease of the plane entropy wave amplitude at the outlet of a stator blade. The streamlines for the stator and the rotor cases are shown in Figs. 11a and b. Using this mean flow quantity (which could be computed by RANS simulations to reduce costs), a delay $t_d(y)$ in arrival of the streamlines at the outlet can be calculated (— in Fig. 12). From this time-delay, Leyko et al. [23] computed the attenuation of the planar mode propagating through the stator,

$$D_0(f) = \left| \frac{1}{l_y} \int_0^{l_y} \exp\left\{2\pi i f t_d(y)\right\} \mathrm{d}y \right|. \tag{58}$$

This attenuation function is displayed in Fig. 13 (—) for the stator stage. The total entropy dissipation of the first mode can be obtained as a convolution product of both rotor and stator transfer functions, which in the frequency domain results in their standard multiplication. The result is shown in Fig. 10 (– – –), as a function of the frequency. It exemplifies that at zero

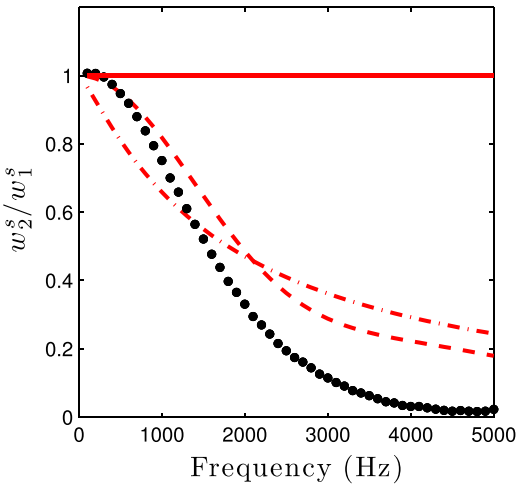

Fig. 10. Entropy transmission through the stator–rotor. —: Analytical theory without attenuation; – – –: Analytical theory with attenuation extracted from the simulation ; – · – · : Analytical theory with a simplified attenuation model ; •: Numerical simulations.

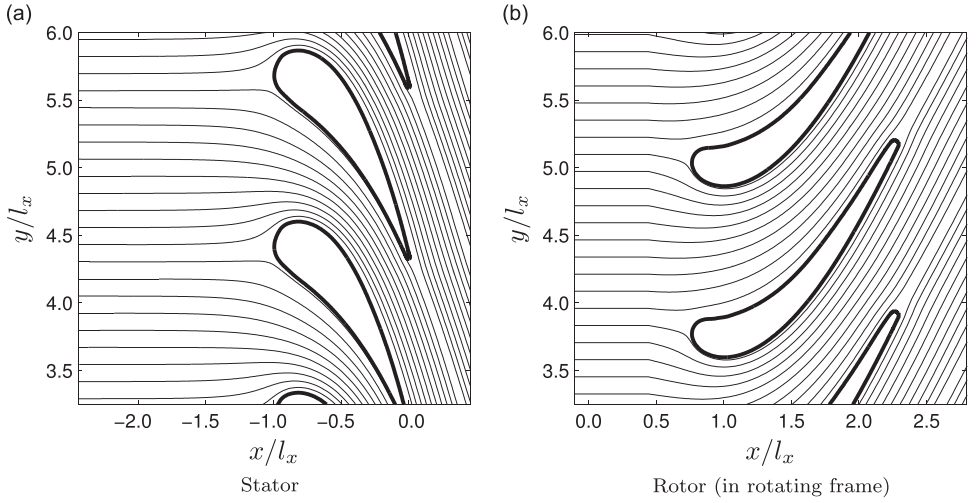

Fig. 11. Streamlines through the turbine blades obtained using the mean flow.

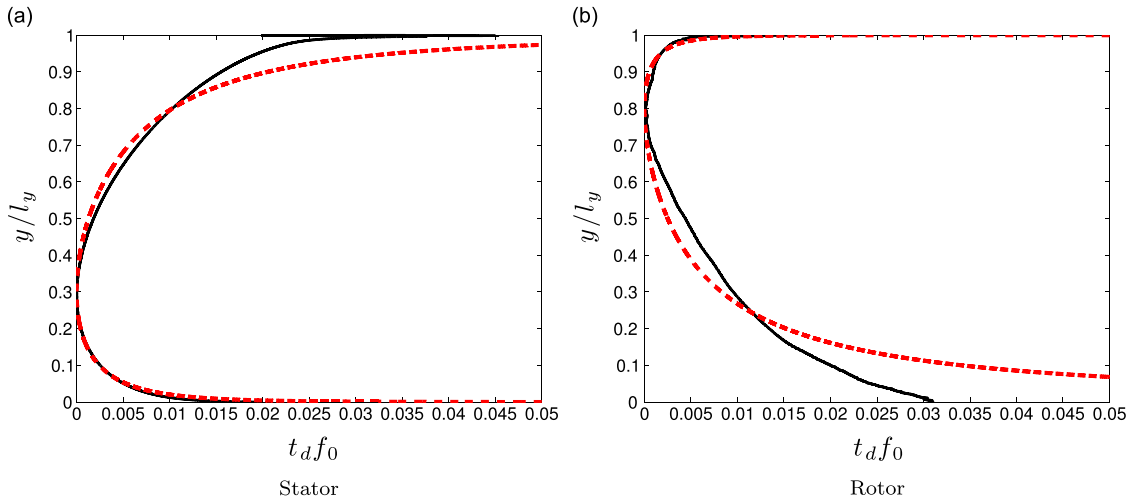

Fig. 12. Time-delay $t_d(y)$ obtained using the LES mean flow (—), and a simplified analytical profile (– – –). Note that $y/l_y = 0$ (respectively $y/l_y = 1$) corresponds to the suction side (respectively pressure side) for the stator blade, and to the pressure side (respectively suction side) for the rotor blade.

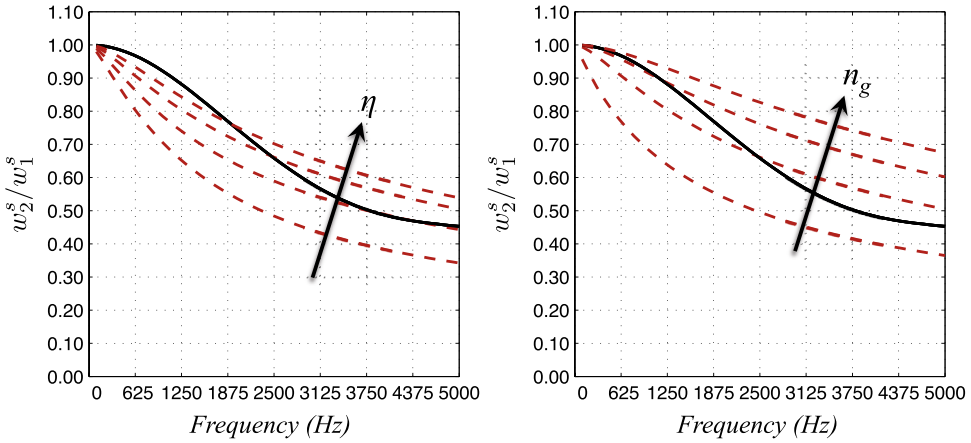

Fig. 13. A parametric study on the asymmetry ($\eta = 0.1$, 0.2, 0.3, and 0.4, left) and flatness ($n_g = 1$, 2, 3, and 4, right) of the velocity profile on the attenuation of the entropy transmission through this single row.

frequency, entropy waves propagate unaltered (no attenuation), but are attenuated for higher frequencies when traveling through the turbine stage: this attenuation model improves the analytical method accuracy. Both transfer functions are injected into the analytical model of Section 2 to provide the entropy transfer functions when considering the entropy dissipation (– – – in Fig. 9). It yields a better agreement with numerical results, especially at high frequencies ($\Omega > 0.1$) where the entropy transmission tends to zero as the frequency increases due to the higher dissipation.

Even though this methodology accounting for entropy attenuation provides overall good results, it requires the knowledge of the delay in arrival time $t_d(y)$, and therefore of the mean flow around each blade. In this study the attenuation function has been obtained using the LES mean field. A drastic cost reduction can be achieved by using RANS simulations, but it would be interesting to have a simple model in which $t_d(y)$ (and therefore $D_0(f)$) could be computed without any numerical simulations. In particular, the question on which parameter controlling the velocity profile affects actually the entropy deformation is still an open topic: typically, the flatness, or the asymmetry of the velocity profile are such potential parameters, for which a generic analytical velocity profile can be used for parametric studies. As an example of such an investigation, the axial mean velocity $\overline{w}_x$ is modeled here along the transverse direction y/l_y using a generic asymmetric power-law, such as

$$\overline{w}_x\left(\frac{y}{l_y}\right) = \left[\frac{y}{l_y}\right]^{\eta/n_g}\left[1-\frac{y}{l_y}\right]^{(1-\eta)/n_g} \tag{59}$$

where η is the asymmetry parameter, controlling the location of the maximum velocity in the profile ($[y/l_y]_{\max} = \eta$), and n_g is the global power of the law. In the present stator–rotor configuration, $n_g^R = 1$ and $\eta_R = 0.8$ for the rotor, and $n_g^S = 2$ and $\eta^S = 0.3$ for the stator. These analytical models are compared with the delay t_d extracted from the simulation in Fig. 12.

Compared with numerical profiles, such theoretical models can be used for parametric studies, for example to analyze the effects of flatness (n_g) or asymmetry (η) on the wave damping function $D_0(f)$.

This model, proposed in Eq. (59), characterizes the mean axial velocity profile at which the entropy spot will propagate through the turbine blade of length l_x. The average mean flow $\overline{w}_x^0 = \frac{1}{l_y}\int_0^{l_y} \overline{w}_x(y/l_y)\, dy$ being known form the operating point, the normalized time delay in arrival time $t_d f_0$ is

$$t_d(y/l_y) = \frac{l_x}{\overline{w}_x^0} \frac{\eta^{\eta/n_g}(1-\eta)^{(1-\eta)/n_g}}{\overline{w}_x(y/l_y)} \tag{60}$$

The time-delay t_d, obtained analytically using Eqs. (59)–(60), is compared with the time-delay extracted from the LES simulation (— in Fig. 12), showing that simple generic profiles with two parameters (flatness and asymmetry) are sufficient to reproduce realistic mean profiles in a turbine stage. The theoretical attenuation function $D_0(f)$ is then computed (Eq. (58)) and injected in the model of Section 2. Predictions of this model for indirect noise (Fig. 9) and entropy transmission (Fig. 10) are compared with cases using (1) no attenuation (—) or (2) a numerical attenuation (– – –). It exemplifies that generic analytical profiles can lead to overall good attenuation predictions, and therefore indirect noise estimations at the design stage.

When varying the asymmetry (η) and flatness (n_g) of the modeled velocity profile, a parametric study of the attenuation function of entropy propagation can be performed, here restrained only to the stator vane for the sake of simplicity. First, the asymmetry is reduced by varying η from 0.1 (corresponding to a very asymmetric case, since η is the location of the maximum velocity in the profile) to 0.4 (almost symmetric case) . As expected, Fig. 13 (left) reveals that reducing the asymmetry of the mean velocity profile (η increases) also reduces the entropy attenuation. Similarly, when increasing the flatness of the velocity profile (n_g increases), the attenuation is also reduced (Fig. 13, right). This simple analysis unveils parameters controlling the attenuation function: when the asymmetry η, or the flatness n_g, increased, they both yield more uniform velocity profiles, and consequently lower attenuation functions. A further analysis is performed in Appendix B to show explicitly the link between the mean axial flow profile and the attenuation behavior with frequency: at low frequency, only the mean velocity deficit is of significant importance, while at higher frequencies, an accurate velocity profile in the boundary layers is required.

This analysis demonstrates that the acoustic and entropy wave propagation and attenuation through a turbine stage can be obtained analytically. It can be generalized for an arbitrary number of stages, as shown in Eq. (49), and therefore be used as a predesign tool for core-engine noise.

5. Conclusions

Because of the modern design of combustion chambers to reduce pollution emissions and the new engine architectures with more compact and highly loaded turbines, combustion noise arouses a novel interest. To complete analytical methods used for acoustic (direct noise) and vorticity wave propagation through a stator vane developed in the seventies, the present study revisits the compact theory proposed by Cumpsty and Marble into a general matrix form, formulation which also takes into account entropy waves to predict indirect noise. A generalization to rotating rows based on the conservation of the rothalpy is proposed to yield a complete propagation model through an entire turbine stage. Consequently, this paper focuses on an analytical model taking into account the propagation of acoustic and vorticity as well as entropy waves through a complete representative turbine stage, containing one stator followed by one rotor.

Such a methodology, termed CHORUS, allows the prediction of energy conversion from entropy to acoustics in a complete stage, leading to indirect noise in a full turbine. In particular, transfer functions characterizing transmission and reflection of waves are obtained analytically, and then compared with numerical predictions from forced compressible Large-Eddy Simulations of a 2D stator–rotor configuration. Numerically, the rotation is addressed by a fluid–fluid coupling strategy with an overset-grid method, termed MISCOG, which has been developed recently and shown to yield good transmission properties in a rotor alone [43]. As expected from the compact assumption in the analytical model, its results agree with the simulation ones at low frequencies only, up to a reduced frequency based on the stator chord length $\Omega \simeq 0.1$. This is mostly the case for the acoustic reflection coefficient and the entropy transmission coefficient. For the acoustic transmission coefficient the frequency range is slightly larger whereas it is narrower for the entropy reflection coefficient. This is consistent with what was found previously by Leyko et al. [23] for a stator vane only.

To improve the indirect noise predictions, the attenuation of entropy spots caused by their deformation through the stator vane or the rotor blade is also considered. As proposed by Leyko et al. [23] it is modeled by time-delays of arrival at the blade outlet, which can be either extracted from the simulations or modeled through an analytical mean axial velocity profile. Even though the latter does not reproduce all the features of the actual distortion in a turbine blade passage, it already includes several parameters that describe the asymmetry (or skewness) and the flatness of this velocity profile. Both the analytical and numerical attenuation improve the indirect noise prediction drastically. Moreover, it is shown in a simple parametric study that the flatness of the mean flow speed and its asymmetry are key parameters controlling the entropy wave attenuation, and therefore indirect noise. A further analysis is developed revealing the link between the mean axial velocity profile and the attenuation behavior with frequency. Results show that at low frequencies, only the mean velocity

deficit is of importance, while at higher frequencies the attenuation is controlled by delay times on arrival in the boundary layers. The complete analytical model already provides a reasonable agreement with 2D simulations, which allows the prediction and minimization of both direct and indirect noise at the design-stage without computation.

Appendix A. Fluctuation of the direction of the relative velocity

For the rotor, the fluctuation of the direction of the relative velocity $(\theta')^r$ has to be related to the fixed reference-frame variables θ' and $w'/\overline{w}$ (Eq. (44)). The sine law in Fig. 2 gives

$$\frac{U}{\sin(\theta-\theta^r)}=\frac{w}{\cos(\theta^r)}, \tag{A.1}$$

which can be differentiated to obtain an equation for the fluctuation of the direction of the relative velocity $(\theta')^r$

$$\left[\theta'-(\theta')^r\right]\cos\left(\overline{\theta}-\overline{\theta}^r\right)=\frac{U}{\overline{w}^2}\left[-(\theta')^r\sin(\overline{\theta}^r)\overline{w}-w'\cos(\overline{\theta}^r)\right]. \tag{A.2}$$

Al-Kashi cosine laws yield

$$\cos\left(\overline{\theta}-\overline{\theta}^r\right)=\frac{(\overline{w}^r)^2+\left(\overline{w}^2-U^2\right)}{2\overline{w}\overline{w}^r}=\frac{\overline{w}^r+U\sin\left(\overline{\theta}^r\right)}{\overline{w}}, \tag{A.3}$$

which allows the simplification of Eq. (A.2) into

$$(\theta')^r=\theta'\left(1+\frac{U}{\overline{w}^r}\sin\left(\overline{\theta}^r\right)\right)+\left(\frac{w'}{\overline{w}}\right)\frac{U}{\overline{w}^r}\cos\left(\overline{\theta}^r\right). \tag{A.4}$$

Appendix B. Effect of the mean axial flow on the attenuation function

The attenuation function $D_0(f)$, to account for the entropy spot distortion through the blades, is based on the delay-time on arrival $\tau_d(y/l_y)$ extracted in the LES or modeled analytically. This function defined in Eq. (58) is recalled here:

$$D_0(f)=\left|\frac{1}{l_y}\int_0^{l_y}e^{2\pi i f\tau_d(y)}\,dy\right|. \tag{B.1}$$

An open question is to understand the effect of the mean axial velocity profile $\overline{w}_x(y/l_y)$, or the time on arrival profile $\tau_d(y/l_y)$, on this attenuation function. The results of the parametric study (Fig. 13) have shown the crucial role of asymmetry η and flatness n_g on the global attenuation level, but explicit relations between $D_0(f)$ and $\tau_d(y/l_y)$ are still required to understand the attenuation behavior with frequency. For instance, knowing which parameters control the attenuation at low and high frequencies, and whether these parameters are identical in both frequency ranges, is a key information to understand mechanisms leading to attenuation and to improve modeling. Writing the exponential function as a power series and using Fubini's theorem to switch the integral–summation order, the attenuation function can be recast as

$$D_0(f)=\left|\sum_{k=0}^{\infty}\frac{(i2\pi f)^k}{k!}\int_0^1\tau_d(y/l_y)^k\,d(y/l_y)\right|=\left|\sum_{k=0}^{\infty}\frac{f^k}{k!}\frac{\partial^k D_0}{\partial f^k}(f=0)\right|. \tag{B.2}$$

Eq. (B.2) reveals explicitly the link between the time on arrival profile τ_d and the behavior of the attenuation function through its derivatives $\frac{\partial^k D_0}{\partial f^k}$. Note that Eq. (B.2) corresponds to a Taylor expansion of $D_0(f)$, and is therefore equivalent to Eq. (58). It can be simplified using only the first N terms of the summation: the truncated relation is then only an approximation of Eq. (58) on the low frequency range $[0,f_N]$, where f_N can be made as large as desired by adding a sufficiently large number of terms N (Fig. 14a).

Nevertheless, compared with Eqs. (58), (B.2) provides some insight on the variation of the attenuation function with frequency. First, the zero-frequency limit is straightforward, since at $f=0$ only the term $k=0$ exists, leading to $\lim_{f\to 0}D_0(f)=1$, which confirms that the entropy spot propagates through the turbine stage without distortion at a null frequency (compact assumption). Second, close to the zero-frequency limit, the behavior of $D_0(f)$ is governed by the term $k=1$, which can be written as $2\pi i f\langle\tau_d\rangle$, where $\langle\tau_d\rangle=\int_0^1\tau_d(y/l_y)\,d(y/l_y)$ corresponds to the mean delay-time on arrival. The slope of the attenuation function at the zero-frequency limit is therefore shown to be only governed by this mean delay time. Moreover, this truncated expression suggests that the behavior of $D_0(f)$ at higher frequencies depends only on the mean quantities $\langle\tau_d^k\rangle$. This result is exemplified in Fig. 14b where the first 26 terms of Eq. (B.2) are displayed for three different frequencies: at null frequency ($f=0$ Hz), at moderate frequencies ($f=2000$ Hz), and finally at high frequencies ($f=4000$ Hz). It indicates that at null frequency ($f=0$), only the mean delay-time on arrival is of significant importance (term $k=1$, since for $k=0$ the coefficient is unity). At moderate frequencies ($f=2000$ Hz), $\langle\tau_d\rangle$ is still dominant, but higher

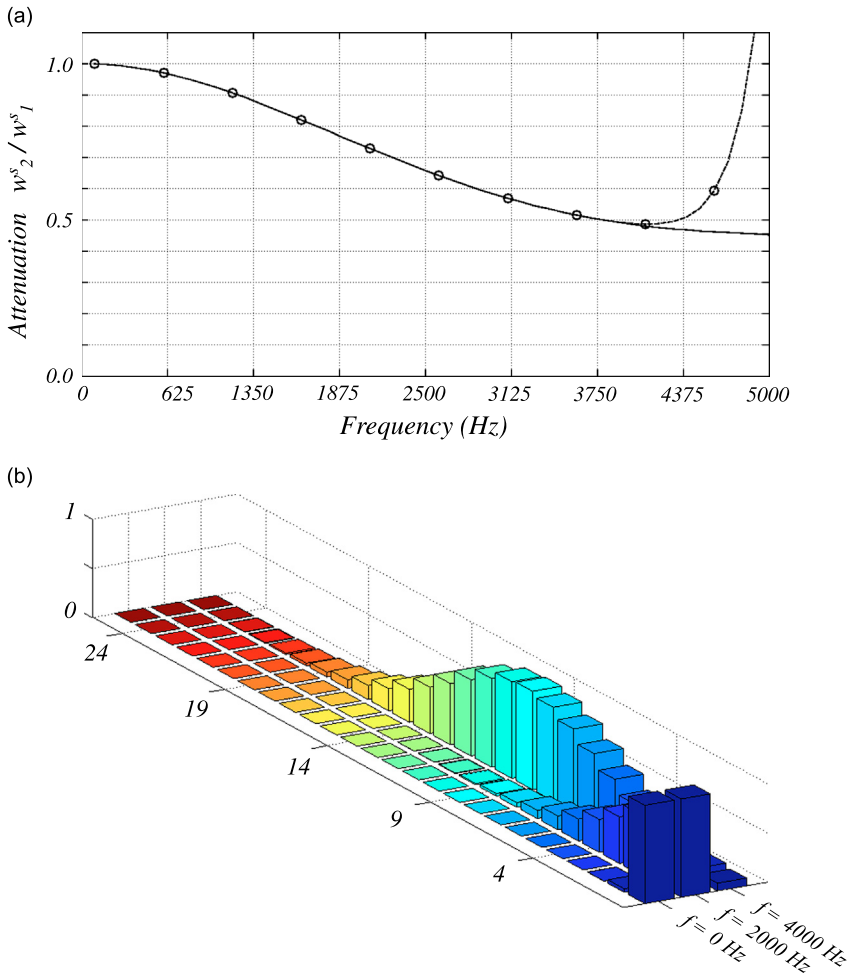

Fig. 14. (a) Attenuation function of the stator extracted from the LES using Eq. (58) displayed by the solid line, and the truncated relation using 26 terms of Eq. (B.2), displayed by a dashed line with circles. (b) Coefficients $(2\pi f)^k \langle \tau_d^k \rangle / k!$ estimated at three different frequencies f: 0 Hz, 2000 Hz, and 4000 Hz for the coefficients $k = 0$–25.

harmonics also appear. Since the mean delay-time $\langle \tau_d \rangle$ is dominant at low frequencies, it shows that the transverse profile is not necessary: only the mean velocity deficit is needed. However, at high frequencies ($f = 4000$ Hz), the mean profile ($k = 1$) does not affect the attenuation anymore. The larger coefficient is found around $k = 9$, meaning that $\langle \tau_d^9 \rangle$ is of significant importance: since τ_d is null near the centerline of the blade, but maximal at walls, it suggests that $\langle \tau_d^9 \rangle$, and therefore the attenuation function at high frequencies, is governed by delay-times in the boundary layers: wall-resolved simulations are mandatory to capture correctly the entropy wave deformation at high frequencies. Typically in the stator case, the whole normalized profile $\{\tau_d / \max(\tau_d)\}^9$ is below 0.001 except in the layer $y/l_y \in [0.975, 1]$.

References

[1] H.M. Atassi, A.A. Ali, O.V. Atassi, I.V. Vinogradov, Scattering of incident disturbances by an annular cascade in a swirling flow, *Journal of Fluid Mechanics* 499 (2004) 111–138.
[2] AVBP code: ⟨http://cerfacs.fr/logiciels-de-simulation-pour-la-mecanique-des-fluides/⟩ and ⟨http://cerfacs.fr/publication/⟩.
[3] F. Bake, C. Richter, B. Muhlbauer, N. Kings, I. Rohle, F. Thiele, B. Noll, The entropy wave generator (ewg): *a reference case on entropy noise*, *Journal of Sound and Vibration* (2009) 574–598.
[4] D. Blacodon, S. Lewy, Source localization of turboshaft engine broadband noise using a three-sensor coherence method, *Journal of Sound and Vibration* 338 (17) (2015) 250–262.
[5] C. Bosman, C.O. Jadayel, A quantified study of rothalpy conservation in turbomachines, *International Journal of Heat and Fluid Flow* 17 (4) (1996) 410–417.
[6] S. Candel, Acoustic transmission and reflection by a shear discontinuity separating hot and cold regions, *Journal of Sound and Vibration* 24 (1972) 87–91.
[7] B.T. Chu, L.S.G. Kovasznay, Non-linear interactions in a viscous heat-conducting compressible gas, *Journal of Fluid Mechanics* 3 (1958) 494–514.
[8] O. Colin, M. Rudgyard, Development of high-order Taylor–Galerkin schemes for unsteady calculations, *Journal of Computational Physics* 162 (2) (2000) 338–371.

[9] N.A. Cumpsty, F.E. Marble, The interaction of entropy fluctuations with turbine blade rows; a mechanism of turbojet engine noise, *Proceedings of the Royal Society of London A* 357 (1977) 323–344.
[10] J. Donea, L. Quartapelle, V. Selmin, An analysis of time discretization in the finite element solution of hyperbolic problems, *Journal of Computational Physics* 70 (1987) 463–499.
[11] I. Duran, Prediction of Combustion Noise in Modern Aero Engines Combining LES Simulations and Analytical Methods, PhD Thesis, INP Toulouse, 2013.
[12] I. Duran, S. Moreau, Numerical simulation of acoustic and entropy waves propagating through turbine blades, *19th AIAA/CEAS Aeroacoustics Conference*, AIAA 2013-2102 paper, Colorado Springs, CO, 2013.
[13] I. Duran, S. Moreau, Solution of the quasi one-dimensional linearized Euler equations using flow invariants and the Magnus expansion, *Journal of Fluid Mechanics* 723 (2013) 190–231.
[14] I. Duran, S. Moreau, T. Poinsot, Analytical and numerical study of combustion noise through a subsonic nozzle, *AIAA Journal* 51 (1) (2013) 42–52.
[15] A. Giauque, M. Huet, F. Clero, Analytical analysis of indirect combustion noise in subcritical nozzles, *Journal of Engineering for Gas Turbines and Power* 134 (11) (2012) 111202.
[16] A. Giauque, M. Huet, F. Clero, Analytical analysis of indirect combustion noise in subcritical nozzles, *Proceedings of ASME TURBO EXPO*, 2012, pp. 1–16.
[17] C.S. Goh, A.S. Morgans, Phase prediction of the response of choked nozzles to entropy and acoustic disturbances, *Journal of Sound and Vibration* 330 (21) (2011) 5184–5198.
[18] M.S. Howe, Indirect combustion noise, *Journal of Fluid Mechanics* 659 (2010) 267–288.
[19] M. Ihme, H. Pitsch, On the generation of direct combustion noise in turbulent non-premixed flames, *International Journal of Aeroacoustics* 11 (1) (2012) 25–78.
[20] S. Kaji, T. Okazaki, Propagation of sound waves through a blade row: *I. Analysis based on the semi-actuator disk theory*, *Journal of Sound and Vibration* 11 (3) (1970) 339–353.
[21] S. Kaji, T. Okazaki, Propagation of sound waves through a blade row: *II. Analysis based on acceleration potential method*, *Journal of Sound and Vibration* 11 (3) (1970) 355–375.
[22] N. Lamarque, T. Poinsot, Boundary conditions for acoustic eigenmodes computation in gas turbine combustion chambers, *AIAA Journal* 46 (9) (2008) 2282–2292.
[23] M. Leyko, I. Duran, S. Moreau, F. Nicoud, T. Poinsot, Simulation and modelling of the waves transmission and generation in a stator blade row in a combustion-noise framework, *Journal of Sound and Vibration* 333 (23) (2014) 6090–6106.
[24] M. Leyko, S. Moreau, F. Nicoud, T. Poinsot, Waves transmission and generation in turbine stages in a combustion-noise framework, *16th AIAA/CEAS AeroAcoustics Conference*, AIAA 2010-4032 paper, Stockholm, Sweden, 2010.
[25] M. Leyko, F. Nicoud, S. Moreau, T. Poinsot, Numerical and analytical investigation of the indirect noise in a nozzle, *Proceedings of the Summer Program*, Center for Turbulence Research, NASA AMES, Stanford University, USA, 2008, pp. 343–354.
[26] M. Leyko, F. Nicoud, T. Poinsot, Comparison of direct and indirect combustion noise mechanisms in a model combustor, *AIAA Journal* 47 (11) (2009) 2709–2716.
[27] M.J. Lighthill, On sound generated aerodynamically. i. General theory, *Proceedings of the Royal Society of London A, Mathematical and Physical Sciences* 211 (1107) (1952) 564–587.
[28] T. Livebardon, Modeling of Combustion Noise in Helicopter Engines, PhD Thesis, INP Toulouse, 2015.
[29] T. Livebardon, S. Moreau, L. Gicquel, T. Poinsot, E. Bouty, Combining les of combustion chamber and an actuator disk theory to predict combustion noise in a helicopter engine, *Combustion and Flame* 165 (2016) 272–287.
[30] F.A. Lyman, On the conservation of rothalpy in turbomachines, *Journal of Turbomachinery* 115 (3) (1993) 520–525.
[31] F.E. Marble, S. Candel, Acoustic disturbances from gas nonuniformities convected through a nozzle, *Journal of Sound and Vibration* 55 (1977) 225–243.
[32] R.S. Muir, The application of a semi-actuator disk model to sound transmission calculations in turbomachinery, part i: *the single blade row*, *Journal of Sound and Vibration* 54 (3) (1977) 393–408.
[33] R.S. Muir, The application of a semi-actuator disk model to sound transmission calculations in turbomachinery, part ii: *multiple blade rows*, *Journal of Sound and Vibration* 55 (3) (1977) 335–349.
[34] M. Muthukrishnan, W.C. Strahle, D.H. Neale, Separation of hydrodynamic, entropy, and combustion noise in a gas turbine combustor, *AIAA Journal* 16 (4) (1978) 320–327.
[35] G.F. Pickett, Core engine noise due to temperature fluctuations convecting through turbine blade rows, *2nd AIAA Aeroacoustics Conference,* AIAA 1975-528 paper, Hampton, VA, 1975.
[36] T. Poinsot, S. Lele, Boundary conditions for direct simulations of compressible viscous flows, *Journal of Computational Physics* 101 (1) (1992) 104–129.
[37] T. Schønfeld, M. Rudgyard, Steady and unsteady flows simulations using the hybrid flow solver avbp, *AIAA Journal* 37 (11) (1999) 1378–1385.
[38] L. Selle, F. Nicoud, T. Poinsot, The actual impedance of non-reflecting boundary conditions: *implications for the computation of resonators*, *AIAA Journal* 42 (5) (2004) 958–964.
[39] S.R. Stow, A.P. Dowling, T.P. Hynes, Reflection of circumferential modes in a choked nozzle, *Journal of Fluid Mechanics* 467 (2002) 215–239.
[40] W.C. Strahle, On combustion generated noise, *Journal of Fluid Mechanics* 49 (1971) 399–414.
[41] W.C. Strahle, Some results in combustion generated noise, *Journal of Sound and Vibration* 23 (1) (1972) 113–125.
[42] C.K.W. Tam, S.A. Parrish, J. Xu, B. Schuster, Indirect combustion noise of auxiliary power units, *Journal of Sound and Vibration* 332 (17) (2013) 4004–4020.
[43] G. Wang, F. Duchaine, D. Papadogianis, I. Duran, S. Moreau, L.Y.M. Gicquel, An overset grid method for large-eddy simulation of turbomachinery stages, *Journal of Computational Physics* 274 (2014) 333–355.
[44] C.S. Yoo, Y. Wang, A. Trouvé, H.G. Im, Characteristic boundary conditions for direct simulations of turbulent counterflow flames, *Combustion Theory and Modelling* 9 (2005) 617–646.